Population genetic structure and hybrid zone analyses for species delimitation in the Japanese toad (*Bufo japonicus*)

Kazumi Fukutani[1], Masafumi Matsui[1], and Kanto Nishikawa[1,2]

[1]Graduate School of Human and Environmental Studies, Kyoto University, Kyoto, Japan
[2]Graduate School of Global Environmental Studies, Kyoto University, Kyoto, Japan

Corresponding Author:
Kazumi Fukutani[1]
E-mail address: fukutani.kazumi.55a@kyoto-u.jp

Abstract

Hybridization following ~~the~~ secondary contact can produce different outcomes, depending on the extent to which genetic diversity and reproductive barriers have accumulated during isolation. The Japanese toad, *B. japonicus,* is distributed on the main islands of Japan. In this study, we applied MIG-seq to achieve a fine-scale resolution on the genetic cluster in *B. j. japonicus* and *B. j. formosus*. Moreover, we elucidated hybridization patterns and gene flow degrees across the contact zones between identified clusters. Using SNP~~s~~ data, we found four genetic clusters in *B. j. japonicus* and *B. j. formosus* and three contact zones of the cluster pairs ~~of~~ among these four clusters. The oldest diverged lineage~~s,~~within *B. j. japonicus* and *B. j. formosus*~~,~~ formed a narrow contact zone consistent with species distinctiveness. Therefore we recommend that these two genetic clusters within these subspecies be elevated to the species level. In contrast, the less diverged pairs of two clusters in *B. j. japonicus* and *B. j. formosus*, respectively, admix over a hundred kilometers, suggesting that they have not yet developed strong reproductive isolation and should be treated as conspecifics. These results contribute to resolving taxonomic confusion in Japanese toads.

Introduction

Hybrid zones are natural laboratories offering many insights into the speciation processes, thus contributing to a better understanding of evolution (Barton & Hewitt, 1985; Hewitt, 1988; Abbott et al., 2013). Hybridization following ~~the~~ secondary contact can produce different outcomes, depending on the extent to which genetic diversity and reproductive barriers have accumulated during isolation. The results are the reduction of differentiation, and fusion of gene pools~~,~~. ~~a~~Alternatively, an increase in the strength of the genetic barrier ~~and~~ can result in complete reproductive isolation (Barton & Hewitt, 1985; Wu, 2001).

Hybridization is frequent and is evolutionarily significant in amphibians. There were well-described studies in amphibians for the hybrid zone ~~in amphibians~~ of fire-bellied toads (*Bombina bombina* and *B. variegata*; e.g., Szymura & Barton, 1986, 1991; Yanchukov et al., 2006), green toads (*Bufotes viridis* subgroups; e.g., Stöck et al., 2006; Colliard et al., 2010; Dufresnes et al., 2014) and more recently those described in the European common toads (*Bufo bufo* and *B. spinosus*; (e.g., Arntzen et al., 2016; Dufresnes et al., 2020; Riemsdijk et al., 2023). Compared to many other anuran species, the Japanese toad, *Bufo japonicus* Temminck and Schlegel, 1838, has the advantage of comprising distinct genetic lineages representing different stages of the speciation process (Fukutani et al., 2022). Moreover, several contact zones of the different genetic lineages have been recognized (Fukutani et al., 2022). For amphibian cases, the extent of natural hybridization in contact zones correlated with divergence times (Hickerson, Meyer & Moritz, 2006; Dufresnes et al., 2021).

Bufo japonicus is widely distributed in the Japanese archipelago, Honshu, Shikoku, Kyushu, and some adjacent islands. This species is divided into two subspecies, *B. j. japonicus* from western Japan and *B. j. formosus* Boulenger, 1883 from eastern Japan. These two subspecies are distributed parapatrically with the boundary in the Kinki region of the central area of Japan (Matsui & Maeda, 2018). Matsui (1984) concluded that *B. j. japonicus* and *B. j. formosus* showed climatic cline in the morphometric characters, which was insufficient to distinguish them as different species because of their identity in the fundamental patterns of modes of life. However, Dufresnes & Litvinchuk (2021) recently proposed elevating *B. j. japonicus* and *B. j. formosus* to the species level, given the Miocene split estimated by mtDNA markers. However, they refrained from taxonomic changes because mitochondrial distances

Commented [DR1]: Are you suggesting that specific clades within these subspecies be elevated, and the other clades not elevated due to the introgression/admixture/hybridization between them? Considering these clades are not likely to be recognizable from one another based off of anything other than genetics (are they morphologically distinct? You mention a morphological cline in the manuscript but are not very specific in the distinction of each clade separately.)
I think that there is evidence that each entire subspecies may be elevated to full species based off of your DAPC plots and your reciprocally monophyletic nuclear clades in your species tree. There are similar cases of toad species delimitation despite mitt-nuclear discordance and introgression in Central and South American toad complexes for reference.
ref:
Firneno TJ Jr, O'Neill JR, Itgen MW, Kihneman TA, Townsend JH, Fujita MK. 2021. Delimitation despite discordance: evaluating the species limits and distributions of a confounding species complex in the face of mitonuclear discordance. Ecology and Evolution 11(18): 12739-12753. https://doi.org/10.1002/ece3.8018

Rivera D, Prates I, Firneno TJ, Rodrigues MT, Caldwell JP, Fujita MK. 2021. Phylogenomics, introgression, and demographic history of South American true toads (Rhinella). Molecular Ecology 31: 978– 992. https://doi.org/10.1111/mec.16280

might not reflect actual species distances. In the other previous studies, it was suggested that the Kinki region might be a hybrid zone of *B. j. japonicus* and *B. j. formosus* by C-banding analysis of chromosomes (Miura, 1995).

The sympatric distribution of mitochondrial haplotypes of *B. j. japonicus* and *B. f. formosus* was also found in the Kinki region (Fukutani et al., 2022). Furthermore, several contact distributions of the genetic lineages in the two subspecies were identified. These studies indicate the necessity of revealing the degree of the hybridization between the two subspecies and other genetic lineages for taxonomic revision. The valid species should exhibit significant divergence and narrow transition zones. In contrast, insufficient diverged lineages that remained conspecific should admix freely across broad genetic areas.

In this study, we applied a multiplexed ISSR genotyping by sequencing (MIG-seq: Suyama & Matsuki, 2015) to achieve a fine-scale resolution on the genetic clusters within *B. j. japonicus* and *B. j. formosus*. Moreover, we elucidated patterns of gene flow and hybridization across the contact zone. MIG-seq has been effectively used to study molecular phylogenetic taxonomy for various taxa (see Suyama et al., 2022). Therefore, we used our results to re-examine the taxonomic status of *B. j. japonicus* and *B. f. formosus*.

Materials & Methods

Sampling and Mig-seq sequencing

A total of 155 samples of *Bufo japonicus* and 13 samples of *B. torrenticola* Matsui, 1976 were collected, covering each distribution (Table S1). The Animal Experimentation Ethics Committee in the Graduate School of Human and Environmental Studies, Kyoto University provided full approval for this research (20-A-5, 20-A-7, 22-A-2). DNA was extracted from frozen or ethanol-preserved tissue samples (e.g., muscles, livers, or skin) with Qiagen DNeasy Blood and Tissue Kit following the manufacturer's instructions.

We prepared two genomic libraries and sequenced them separately for the convenience of the experiment, and the data obtained were analyzed together as described below. Library 1 included 121 samples of *Bufo japonicus* and 13 samples of *B. torrenticola*, and library 2 had 40 samples of *B. japonicus*, with six samples of *B. japonicus* overlapping in both libraries (Table S1). The two genomic libraries were prepared following the protocol described in Matsui et al. (2019) for library 1 and the protocol described in Watanabe et al. (2020) for library 2. The libraries 1 and 2 amplicons were purified and sequenced on the Illumina MiSeq Sequencer (Illumina San Diego, CA, USA) using a MiSeq Reagent Kit v3 (150 cycles, Illumina). For the convenience of the molecular experiment, two libraries were prepared and sequenced separately, and the obtained raw sequence data were combined for subsequent data analysis.

Raw sequence reads of the Mig-seq data were deposited in the DNA Data Bank of Japan (DDBJ) Sequence Read Archive (DRA) under accession number DRA016475 (BioProject ID; PRJDB15971: BioSample ID; SAMD00622809–SAMD00622982).

The raw paired-end sequences (reads 1 and 2) were filtered by fastp version 0.23.2 (Chen et al., 2018) to trim the first 14 base sequences of read 2 and primer region of read 1 and 2 and to discard the reads shorter ~~reads~~ than 80 bp and the low-quality sequences with phred quality Q < 30 according to Suyama and Matsuki (2015). Then, we mapped the filtered reads to the reference sequencing because ~~the~~ mapping can obtain more loci than de novo analysis for the MIG-seq data (Takata et al., 2021). ~~As~~ For the reference genome sequence for Japanese toads, we used the genome assembly of their closely related species, *B. gargarizans* (RefSeq assembly accession number: GCF_014858855.1; https://www.ncbi.nlm.nih.gov/data-

hub/genome/GCF_014858855.1/). The assembly contained a total of 11 chromosome-level contigs and unplaced scaffolds. Finally, we mapped the filtered reads to the indexed reference sequencing by bwa-mem2 version 2.2.1 (Vasimuddin et al., 2019) to make SAMfiles which were converted to BAM files and sorted with a minimum mapping quality of 20 using *samtools* version 1.15 (Li et al., 2009).

Genotyping

We prepared the following datasets: i) data from the samples of *B. japonicus* and *B. torrenticola* to explore the genetic structure of Japanese toads, and ii) Data from the samples of *B. j. japonicus* and *B. j. formosus* to investigate the degree of reproductive isolation between the two subspecies. For these two datasets, we excluded the 11 samples considered to be from the artificially introduced population. Instead, we prepared a dataset iii) including these 11 samples with dataset ii) to verify the population's genetic assignments of them.

The reference-based analysis pipeline with the *gstacks* program followed by the *populations* program in Stacks v2.60 (Rochette, Rivera-Colón & Catchen, 2019) was applied to the mapped reads of all data sets to call SNPs and genotypes. The following filters were used for the *populations* program in Stacks. First, we keep variant sites with a minimum allele count of three (--min-mac 3) to ensure an allele is in at least two diploid samples (Rochette, Rivera-Colón & Catchen, 2019). Second, we set up the maximum observed heterozygosity at 0.5 (--max-obs-het 0.50) because the heterozygosity for a biallelic SNP is expected < 0.5, and SNPs with values above this threshold may belong to paralogous loci or multilocus contigs (Hohenlohe et al., 2011; Willis et al., 2017). Third, only one random SNP per locus was extracted (--write-random-snp) to avoid any influence of linkage among SNPs on the multivariate analysis (Gargiulo, Kull & Fay, 2020). For the population designation in a populations map, we set two populations corresponding to *B. japonicus* and *B. torrenticola* for dataset i). For datasets ii) and iii), we set two populations based on the *q*-value (with *q*-value = 0.5 as a boundary) at the optimal number of clusters (*K*) = 2 of Structure analysis (see below; Pritchard, Stephens & Donnelly, 2000) on dataset i). Finally, we processed only the loci presented in at least 80% of samples in a population (*-r* = 0.80) and that presented in two populations for all datasets (*-p* = 2). For the following stacks program, the two parameters, *-r* and *-p*, were varied, and the others were common for each analysis.

Estimation of the genetic structure

To estimate the population genetic structure of *B. japonicus* and *B. torrenticola*, we performed three different methods using the SNP genotyping information and compared grouping among these methods: discriminate analysis of principal components (DAPC; Jombart, Devillard & Balloux, 2010), Structure 2.3.4 (Pritchard, Stephens & Donnelly, 2000), and principal components analysis (PCA; Cavalli-Sforza, 1966).

DAPC was performed on dataset i) in the R package *adegenet* 2.1.8 (Jombart, 2008; Jombart, Devillard & Balloux, 2010; Jombart & Ahmed, 2011). This method maximizes the variance among groups while minimizing the variation within groups without making assumptions about the underlying population genetic model. This approach transforms multilocus genotype data using PCA to derive the uncorrelated variables that are input for discriminate analysis. First, the optimal groups were assessed using the de novo clustering method, *find.cluster*, testing *K* values from 1 to 8, and the best *K* value was chosen with the Bayesian information criterion (BIC) method. This de novo clustering method and an initial

DAPC using the *dapc* function were run, after which the *optim.a.score* was used to assess the optimal number of principal components (PCs) to retain. Once the optimal number of PCs was determined, a second DAPC analysis was conducted using this value.

The program Structure 2.3.4 (Pritchard, Stephens & Donnelly, 2000) performed the analysis by an admixture model with correlated allele frequencies based on the Bayesian clustering method to infer the population structure. Because excessive uneven sampling likely increases the bias on the admixture proportions of Structure analysis (Toyama, Crochet & Leblois, 2020), we reduced the sample size in Yakushima and Tanegashima from dataset i) ~~as~~ (called dataset i)-2 and conducted the Structure analyses. Structure analyses were carried out for the number of clusters *K* from 1 to 8, with ten runs for each *K* value. Markov chain Monte Carlo (MCMC; Metropolis et al., 1953; Hastings, 1970) iterations of 100,000 were implemented for each run after an initial burn-in of 100,000. The parallelization of Structure 2.3.4 calculations was achieved using EasyParallel (Zhao et al., 2020) to reduce computational time. The optimal number of clusters was inferred in StructureSelector (Li & Liu, 2018) with the Delta *K* (ΔK; Evanno, Regnaut & Goudet, 2005), MedMeaK, MaxMeaK, MedMedK and MaxMedK (Puechmaille 2016). StructureSelector integrated the CLUMPAK program (Kopelman et al., 2015) to cluster and merge data from independent runs and generate graphical representations of the results. In Structure analysis, admixed ancestry is modeled by assuming that an individual has inherited some proportion (*q*-value) of its genome from ancestors in the population (Pritchard, Stephens & Donnelly, 2000).

PCA was performed on dataset i) using the R package *adegenet* 2.1.8 (Jombart, 2008; Jombart & Ahmed, 2011), and the first two eigenvectors were plotted in two dimensions.

Moreover, we conducted Structure analysis on dataset iii) to identify the assignment of genomic clusters for the samples from introduced populations, reducing the sample size in Yakushima and Tanegashima for the above reason as dataset iii)-2. Structure analysis was carried out for the number of clusters *K* from 1 to 6, and other parameters were the same as above.

Estimate the phylogeny

We used SNAPP 1.5.2 (Bryant et al., 2012) implemented in Beast v 2.6.7 (Bouckaert et al., 2019) to estimate the phylogenetic relationships among populations identified by our clustering. We chose four individuals for each population and applied them to the stacks program (*-r* = 1.0 and *-p* = 5). We ran SNAPP for 10,000,000 iterations with mutation rates *u* and *v* = 1.0, a gamma distribution with *alpha* = 2 and *beta* = 200 for the lambda prior, and *alpha* = 1, *beta* = 250, *kappa* = 1, and *lambda* = 10 for the *snapprior*, sampling every 1,000 steps. The convergence was examined using Tracer 1.7.2 (Rambaut et al., 2018), and the result was visualized by Densitree 2.2.7 with a burn-in of 10%. The maximum clade credibility tree with posterior probability was calculated using TreeAnnotator version 2.6.7 (Bouckaert et al., 2019). To compare, we reconstructed the mitochondrial phylogenetic tree using the mitochondrial cytochrome *b* sequences from Fukutani et al. (2021) of the same individuals used for constructing the SNP tree adding the sequence of *B. g. gargarizans* as the outgroup. RAxML version 8.2.12 (Stamatakis, 2014) was employed for 1,000 bootstrap iterations with the GTRGAMMA model to infer a maximum likelihood phylogenetic tree based on the mitochondrial sequences.

Effective estimates of migration surfaces

We visualized spatial patterns of gene flow using FEEMS (Fast Estimation of Effective Migration Surfaces; Marcus et al., 2021) to assess the genomic context and geographic location of any historical barriers to migration in *B. japonicus*. FEEMS is an improvement of EEMS (Estimated Effective Migration Surfaces; Petkova, Novembre & Stephens, 2016) and uses a Gaussian Markov Random Field model in a penalized likelihood framework. This method uses locality information and pairwise dissimilarity matrices calculated from SNP data to identify regions where genetic similarity decays more quickly than expected under isolation by distance (Petkova, Novembre & Stephens, 2016). To estimate effective migration parameters, we used as inputs the genotype data of dataset ii), as well as the coordinate information of each individual. A polygon grid was prepared using QGIS 3.28. Finally, cross-validation was performed, and the lambda with the lowest cross-validation value was used to generate the final plot.

Hybrid zone analyses

To estimate the geographic gradient of genomic differences between adjacent clusters of *B. japonicus*, we calculated the steepness of the cline of the genetic differences. Cline analyses could explain the transition between characters of interbreeding species across the hybrid zone and contribute to the understanding of the mechanisms maintaining species boundaries (Barton & Hewitt, 1985). Assuming similar dispersal abilities among the individuals of each cluster, and no geographic barriers to gene flow at their transitions, wide hybrid zones will be present for the younger pairs can be estimated if they did not yet evolve significant reproductive isolation, whereas narrow transitions will be present for the older pairs if they represent distinct species.

We fitted clines to the nuclear ancestry (Structure *q*-value) and some mitochondrial haplogroup frequency data from our previous study (Table S1; Fukutani et al., 2022) across the geographic transition between the genetic clusters identified in our study area using the R package *hzar* version 0.2-7 (hybrid zone analysis using R; Derryberry et al., 2014). The shape of each cline is modeled by combining three equations (Szymura and Barton 1986, 1991) that describe a sigmoid shape at the center of a cline (maximum slope) and two exponential decay curves on either side of the central cline (tails).

We reduced two-dimensional space (latitude and longitude) into a single-dimensional distance from the hybrid zone for *hzar*. The probable center line of admixture was estimated using R package *tess3r* version 1.1 (Caye, 2016, 2018), considered the baseline for *hzar*, and calculated the minimum distances from the baseline to individuals in QGIS 3.28. We assigned a positive or negative sign to these distances depending on individual orientation to the baseline of admixture.

Admixture proportions inferred by the Structure program (Pritchard, Stephens & Donnelly, 2000) have often been used to fit a geographic consensus cline, from which the width of the hybrid zone is estimated (e.g., Tominaga et al., 2018; Dufresnes et al., 2020b). As before, to avoid bias on the admixture proportions of Structure, we also reduced the sample size in Yakushima and Tanegashima from dataset ii).

We performed the stacks program on this subset setting four populations based on the results of DAPC on dataset ii), with *-r* = 0.80 and *-p* = 4, and conducted Structure analysis using the parameters same as above. This subset was divided into three sub-datasets i), ii), and iii), based on the *q*-value at $K = 4$ with some samples overlapped. Each sub-dataset contained individuals of two pure clusters, considering *q*-value > 0.90 as pure individuals and admixtured individuals between pure clusters. We applied the stacks program for each sub-datasets, setting three populations (two pure and one admixtured population) with *-r* = 0.80 and *-p* = 3, and

conducted Structure analysis. The q-values on $K = 2$ for each sub-dataset were used to perform *hzar*. In addition to the three sub-datasets, we prepared sub-datasets iii)-2, which is the data excluding samples in Shikou and Seto Inland Sea (see discussion), and performed the analysis in the same way as for the other sub-dataset.

We tested 15 different models for each cline, plus a null model with no cline, running the MCMC algorithm and using the Akaike information criterion score corrected for a small sample size (AICc; Anderson & Burnham, 2002).

These 15 models combined three trait intervals and five fitting tails. The three possible combinations of trait intervals were used to scale clines by the minimum (p_{min}) and maximum (p_{max}) values in the cline: no scale (fixed to $p_{min} = 0$ and $p_{max} = 1$), observed values (fixed to p_{min} = minimum observed mean values, p_{max} = maximum observed mean values), and estimated values (p_{min} and p_{max} as the free parameter). The five possible combinations of fitting tails represent the cline shapes: no tails, right tail only, left tail only, symmetrical tails, mirror tails, and both tails estimated separately.

The MCMC was performed for each model with the default values of 100,000 generations, each with a randomly selected seed and 10% of steps discarded as a burn-in. After each run, we compared the model performance using the AICc. The model with the lowest AICc score was chosen as the best-fit model to infer cline widths and centers along with a 95% confidence interval. The stability and convergence of the cline parameters of the best-fit model were assessed by visualizing MCMC traces. We plotted the maximum-likelihood clines and 95% credible cline region for the best-fit model.

Introgression

We assigned individuals in each contact zone to hybrid classes to estimate whether gene flow is an ongoing or historic admixture. First, we temporarily designated individuals with q-values > 0.98 for the $K = 2$ in Structure analysis on sub-datasets iv), v), and vi) as parental individuals for each cluster following Scordato et al. (2017). We identified ancestry-informative markers by calculating AMOVA F_{ST} for SNP between pairs of parental clusters using the stacks program on the sub-datasets, setting three populations (two parental and one admixtured population) and *-r* = 0.80 and *-p* = 3. The diagnostic loci, $F_{ST} = 1$, were selected as ancestry-informative markers segregating between each pair of parental clusters.

We used the R package INTROGRESS version 1.2.3 (Gompert & Buerkle, 2010) to calculate maximum-likelihood estimates of the hybrid index for each individual and the average heterozygosity of each individual across informative loci. We compared genomic hybrid indices with heterozygosity to determine the individual hybrid classes. Pure individuals were defined by a hybrid index of 0 or 1 because only the loci fixed in parental individuals with F_{ST} =1 were used. The first-generation hybrids (F1) have an expected hybrid index of 0.5 and heterozygosity of 1.0. We considered individuals with intermediate hybrid indices (> 0.25 and < 0.75) and high heterozygosity (≥ 0.5) as recent-generation hybrids, with intermediate hybrid indices (> 0.25 and < 0.75) and low heterozygosity (< 0.5) as later-generation hybrids, and with low hybrid indices (≤ 0.25 or ≥ 0.75) as backcross to one or the other parental type following previous studies (Milne & Abbott, 2008; Scordato et al., 2017; Slager et al., 2020).

Estimation of the migration rates

Lastly, recent migration rates between parental and hybrid populations were calculated using the Bayesian inference approach by BayesAss3-SNPs v 1.1 (Wilson & Rannala, 2003; Mussmann et

al., 2019). Using the sub-dataset i), ii), and iii) after applying ~~for~~ the stacks program with each setting for three populations (two parental and one admixtured population) and *-r* = 0.80 and *-p* = 3, BA3-SNPs -autotune v2.1.2 (Mussmann et al., 2019) was performed with the default parameters to find the mixing parameters for BA3-SNPs. BayesAss3-SNPs was conducted with ten million generations sampling every 100 generations using the predefined mixing parameters. The first one million generations were discarded as a burn-in, and the chain convergence was assessed in Tracer v 1.7.2 (Rambaut et al., 2018).

All analyses by R were conducted in R studio version 2022.07.2.576 (Rstudio Team 2022) using R version 4.2.2 (R Core Team 2022).

Results

Mig-seq analyses data

A total of 46,889,160 clean reads in 168 samples passed the quality filtering, with the average percentage of reads that passed filtering for each sample being 77.6%. Among them, 17,644,888 reads were successfully mapped to the reference genome of *B. gargarizans* in the reference-mapping approach with an average mapping quality of 27.2%.

Population structure

A total of 839 variants were identified in dataset i) of 157 samples of *B. japonicus* and *B. torrenticola*.

We retained ~~keeping~~ all of the information (157 PCs) for the initial DAPC on dataset i). After running the initial steps, the first 21 PCs were retained following the result of the *optim.a.score* function (Fig. S1A). The BIC plot in DAPC displayed the lowest value at $K = 4$ and 5 (Fig. S1B), and both clearly identified three clusters corresponding to *B. j. formosus*, *B. j. japonicus,* and *B. torrenticola*. The results of $K = 4$ identified two subclusters within *B. j. japonicus*. In addition to that, two subclusters within *B. j. formosus* were recognized for $K = 5$, but these defined subclusters within *B. j. japonicus* and *B. j. formosus* had substantially overlapped plotts between subclusters (Fig. 1A).

A total of 570 variants were identified in dataset i)-2 of 131 samples. A Structure analysis on dataset i)-2 supported two peaks for ΔK estimation, $K = 2$ and 5 (Fig. S2A), and the number of K estimated from MedMeaK, MaxMeaK, MedMedK, and MaxMedK values was 5 (Fig. S2B). Therefore $K = 5$ can be the valid cluster number in our result, resulting in a similar grouping pattern to the DAPC (Fig. 1B). The five genetic clusters identified by DAPC and Structure analyses corresponded to northern *B. j. formosus* (NF), southern *B. j. formosus* (SF), eastern *B. j. japonicus* (EJ), western *B. j. japonicus* (WJ) and *B. torrenticola*. The cluster assignments for individuals by DAPC are shown in Table S1.

The Structure bar plot revealed that *B. torrenticola* has rare admixtures with *B. japonicus*, three samples of *B. torrenticola* had the *q*-values from 0.85 to 0.9, and one sample of *B. j. formosus* had a *q*-value of 0.09 admixed with *B. torrenticola*. These samples are likely hybrid individuals based on the *q*-value threshold following Vähä & Primmer (2006). Therefore, the one admixed sample of *B. j. formosus* was excluded from the following analysis on the *B. japonicus*.

Structure assignments also revealed hybridization between each adjacent cluster of *B. japonicus* (Fig. 1B). The proportion assignment for each cluster of *B. japonicus* changed in steps. High levels of continuous admixture were indicated across the geographic transition between NF and SF and between EJ and WJ, while the hybrid individuals were limitedly confined at the boundary between SF and EJ.

In PCA, the first PC axis explained 25.1% of the genomic covariance and separated the two subspecies, *B. j. formosus* and *B. j. japonicus* (Fig. 1C). By the second PC axis, *B. torrenticola* was clearly split from *B. japonicus*. In addition, the second axis separated two continuous clusters within *B. j. japonicus*.

Artificially introduced population

A total of 718 variants were identified in the 128 samples of dataset iii)-2, *B. japonicus,* including the 11 samples from the artificially introduced populations in Hokkaido, Izu Islands, and the Kanto region. Two individuals in Hokkaido (Asahikawa and Hakodate) had an admixture, mainly two clusters of NF and SF, similar to those in Niijima and Kouzushima (Fig. S3). Individuals in Tokyo and Kanagawa prefectures had admixtured four clusters of NF, SF, EJ, and WJ. The individual in Oshima had three clusters of SF, EJ, and WJ, and one in Hachijojima had SF and EJ clusters.

Species tree

The phylogeny based on five clusters recovered all mitochondrial splits (Fukutani et al., 2022) but the most recent one, northern and southern Tohoku region (Fig. 2). However, the topology based on SNP conflicted with the mitochondrial tree for the clades in western Japan. The EJ and WJ clusters were derived as sister lineages, while mitochondrial topology showed that the EJ and *B. torrenticola* were sister lineages leading to the paraphyly of *B. j. japonicus*.

Commented [DR2]: It would be useful to indicate how many SNPs this tree is based off of.

Effective estimates of migration surfaces

A total of 783 variants were identified in the dataset ii) 143 samples of *B. j. japonicus* and *B. j. formosus*. The estimated effective migration rates evidenced low migration rates between *B. j. formosus* and *B. j. japonicus* despite the absence of any geographic barrier that limits gene flow between subspecies (Fig. 3). Among *B. j. japonicus*, low migration rates were detected between Chugoku and Shikoku vs. Kyushu, and Kyushu vs. Yakushima, likely due to the presence of straits. In contrast, high migration rates were detected within them. On the other hand, among *B. j. formosus*, low migration rates were widely identified from Tohoku to Chubu, likely due to less interaction between regions than among *B. j. japonicus*.

Hybrid zone analyses

Each sub-dataset consisted of cluster pairs, sub-datasets i) NF–SF of 47 samples, ii) SF–EJ of 47 samples, and iii) EJ–WJ of 59 samples. The geographic distribution of each cluster detected by *tess3r* on each sub-dataset ($K = 2$) was not different from that of Structure analyses by SNP data. The baselines across the three contact zones are shown in Fig. 4. There were two best-supported models in *hzar* with the lowest AICc score. One model (model 1) was that scaling was fixed to the minimum value of 0 and maximum value of 1, and no exponential tails were desired for SNP data of sub-dataset SF–EJ and mtDNA data of EJ–WJ. The other model (model 2) was that the scaling was fixed to the minimum and maximum observed mean values, and no exponential tails were desired for SNP data of sub-datasets NF–SF and EJ–WJ and mtDNA data of SF–EJ and NF–SF.

Based on the SNP data, the cline width decreased from NF–SF 170 [CI (95% confidence interval): 82–362] km to EJ–WJ 162 (CI: 63–330) km, SF–EJ 29 (CI: 24–76) km (Fig. 5). The estimated center based on SNP data as the distance from the baseline were 0.6 (CI: -9.5–12) km for SF–EJ, 5.4 (CI: -42–58) km for NF–SF, and 7.0 (CI: -40–56) km for EJ–WJ.

Based on the mtDNA data, the cline width decreased from NF–SF 86 [CI (95% confidence interval): 35–223] km to EJ–WJ 75 (CI: 31–212) km, SF–EJ 39 (CI: 18–106) km(Fig. 5). The estimated center based on mtDNA data as the distance from the baseline were 0.3 (CI: -12–15) km for SF–EJ, 23 (CI: -12–64) km for NF–SF, and -33 (CI: -75–-6.2) km for EJ–WJ.

In addition, for the sub-datasets iii)-2 EJ–WJ excluding Shikoku and Seto Inland Sea, model 2 was selected for SNP and mtDNA data. Based on the SNP data, the width was 99 (CI: 33–301) km, and the distance from the baseline was -1.2 (CI: -38–53) km, and based on the mtDNA data, the width was 79 (CI: 32–245) km and the distance from the baseline was -33 (CI: -76–-2.0) km (Fig. 5).

Introgression

We identified loci that were informative for assigning hybrid classes for each sub-dataset. There were 40 loci with $F_{ST} > 1.0$ between parental SF and EJ, and six loci for NF and SF pair and EJ and WJ pair. Comparing individual hybrid indices and average heterozygosity using these differentiated loci revealed that none of the pairs contained F1 individuals (Fig. 6). The recent-generation hybrids with high heterozygosity were detected only in NF–SF contact zone, confirming ongoing gene flow. The later-generation hybrids were detected in all contact zones, and the hybrid individuals with intermediated hybrid index values and heterozygosity of zero were identified in NF–SF and EJ–WJ contact zones, suggesting the old-origin hybrids survived. The backcrossed individuals with both parental populations were identified in NF–SF and SF–EJ contact zones, while those with one parental population were in EJ–WJ contact zone.

BayesAss directional migration

The mixing parameters for migration rates (*-m*), allele frequencies (*-a*) and inbreeding coefficients (*-f*) were determined by BA3-SNPs-autotune for each sub-dataset: sub-dataset NF–SF, *-m* =0.2125, *-a* =0.55, *-f* =0.1; SF–EJ, *-m* = 0.2125,*-a* =0.55, *-f* =0.1281; EJ–WJ, *-m* = 0.1563, *-a* =0.325, *-f* =0.1.

All estimated migration rates between populations are shown in Table 1. For the sub-dataset NF–SF, the self-recruitment estimate of the parental population of SF was high at > 95%, while that of the parental population of NF and hybrid population are shown to be slightly low (90–95%). The northward migration rates through the hybrid zone, from the parental SF to the hybrid (5.9%) and from the hybrid to the parental NF (3.6%), were higher than the opposite direction migration rates, from the parental NF to the hybrid (1.5%) and from the hybrid to the parental SF (1.7%).

For the sub-dataset SF–EJ, the self-recruitments within both parental populations were estimated to be high at > 95%. In contrast, the hybrid population had low self-recruitment rates at 76.2%. Correspondingly, the outward migration rates from the hybrid population into parental populations were relatively low (2.0% to parental SF and 1.3% to parental EJ efflux). In contrast, the migration rates into hybrid populations were high (16.7% from parental SF and 7.1% from parental EJ influx).

For the sub-dataset EJ–WJ, the self-recruitment of both parental populations was high at > 95%, and that of the hybrid population was intermediate value at 80.1%. The estimations of migration rates from hybrid into both parental populations were relatively low (1.3% to parental EJ and 1.4% to parental WJ efflux), while the migration rates into hybrid populations were high

(7.3% from parental EJ and 12.6% from parental WJ influx). The migration rates among each parental population were estimated to be very low, ranging from 1.3% to 2.6%.

Discussion

Genetic clustering and phylogeny

The previous study showed that Japanese toads diverged into six mitochondrial lineages from the late Miocene to the middle Pleistocene (Igawa et al., 2006; Fukutani et al., 2022). Especially the two subspecies, *B. j. japonicus* and *B. j. formosus,* were recommended to elevate to species level given their Miocene split. However, these previous studies were insufficient for the taxonomic conclusion because they were based on only mitochondrial analyses (Dufresnes & Litvinchuk, 2021). Given the contact distribution of the two subspecies (Fukutani et al., 2022) and the possible presence of a hybrid zone between them (Miura, 1995), identifying the status of the hybrid zone is necessary for the systematic study of Japanese toads. First, we used SNP markers with samples covering virtually the complete distribution ranges of *B. j. japonicus*, *B. j. formosus*, and *B. torrenticola* and presented the clustering and phylogenetic relationship between the identified clusters. Second, this study presents a fine-scale analysis of gene flow across secondary contact zones of *B. j. formosus* and *B. j. japonicus*.

The consensus across independent methods suggests that $K = 5$ best describes the population structure of *B. japonicus* and *B. torrenticola*. This SNP clustering was roughly concordant with the five main mitochondrial clades in Fukutani et al. (2022), except for the lesser diverged mitochondrial clade in the Tohoku region. However, the topology of SNP was discordant with the mitochondrial phylogenetic topology. The SNP phylogenetic tree showed EJ and WJ as sister clades and supported the monophyly of *B. j. japonicus*. However, in the mitochondrial phylogenetic tree, *B. j. japonicus* was paraphyletic since *B. torrenticola* and WJ were identified as sister clades with a high node support (Fig. 2). One explanation is that *B. torrenticola* and the ancestor of EJ and WJ all diverged simultaneously. Alternatively, the discordance may stem from ancestral mitochondrial introgression between *B. torrenticola* and WJ after they diverged. These hypotheses could be tested explicitly in future phylogenetic studies.

The hybrid zone between *B. j. japonicus* and *B. j. formosus*

We found mitochondrial, and SNP marker cline positions and shapes vary for three contact zone and different patterns of gene flow. First, the hybrid zone between *B. j. formosus* and *B. j. japonicus* showed a sharp genetic transition, with concordant and coincided clines between mtDNA and SNP (Fig. 5).

The cline width depends, in part, on whether the hybrid zone is structured primarily by selection or by a neutral process (Mallet et al., 1990). The cline width without any form of selection can be calculated using the diffusion approximation from Barton & Gale (1993), $w = 2.51\sigma\sqrt{T}$, where w, cline width, T, number of generations since secondary contact, and σ, average lifetime dispersal. While the lifetime dispersal distance for *B. japonicus* is unknown, the maximum dispersal distance recorded for native *B. j. formosus* between the breeding pond and the summer home range is 0.26 km, and the generation time is three years (Kusano, Maruyama & Kaneko, 1995). At a dispersal of 0.78 km per generation, cline width exceeds the 29.4 km width of the hybrid zone in ca. 677 years of unrestricted diffusion. Considering their paleo distribution, they contacted with expansion after the last glacial period at the latest (Fukutani et al., 2022). Therefore, the contact between the subspecies is arguably much older than 677 years

ago. The cline width may have been kept narrow over a long time despite no geographic barriers to dispersal, presumably through selection against hybrids, suggesting that the two subspecies form a tension zone (Key, 1968) in the Kinki region. In addition, all hybrid individuals were classified by INTROGRESS as layer-generation hybrids or backcrosses, suggesting the relatively ancient origin of their contact.

Taxonomic revision of *B. japonicus*

Our result showed that hybridization persists over time as parentals move into the hybrid zone (Table. 1), while introgression is limited by negative selection against hybrids, allowing species to maintain their genetic distinctiveness (Barton and Hewitt 1985). These results thus call for a taxonomic revision of *B. japonicus*. Therefore, we now consider the eastern Japanese common toad *Bufo japonicus formosus* Boulenger, 1883 as a distinct species previously considered a subspecies of the western Japanese common toad *Bufo japonicus* Temminck and Schlegel, 1838. However, the previous study did not find intermediate forms in the Kinki region, and the morphological boundary extended more westerly to the Chugoku region (Matsui, 1984). The discordant patterns in morphological and genetic markers can be due to various factors worth further exploration.

Speciation with gene flow is common in anurans (Dufresnes et al. 2021). For example, the study on two European *Bufo* species, *B. bufo* and *B. spinosus*, which diverged in the Late Miocene, showed limited gene flow across a narrow hybrid zone (about 30 km width) in the northwest of France despite no barriers to dispersal (Arntzen et al., 2016). Despite the presence of a hybrid zone for *B. formosus* and *B. japonicus*, the identity of the parental species is distinctive and seems to have been unaffected. These two species could be considered to remain in partial reproductive isolation over a long period (Servedio and Hermisson, 2020). Cline coupling may have progressed further toward reproductive isolation after secondary contact, and it could still be ongoing throughout the hybrid zone (Harrison & Larson, 2014; Butlin & Smadja, 2018).

We also found that the geographic location of the hybrid zone between the two species is likely environment-independent. The ecological niche modeling in Fukutani et al. (2022) showed that environmental conditions are suitable for both species across the hybrid zone identified in this study, suggesting that environment-associated selection may not act directly to keep the hybrid zone. It is known that the many anuran speciation processes initiate through a gradual accumulation of multiple barrier loci scattered across the genome, which reduces hybrid fitness by intrinsic postzygotic isolation (Dufresnes et al., 2021). Similarly, for *B. formosus* and *B. japonicus*, it is possible that many genomic regions experience local barriers to gene flow and maintain steep and coincide clines rather than exogenous selection. We could identify the genomic mechanism that induced the speciation in future studies.

The hybrid zone within *B.j japonicus*

Given the refugia distributions in Fukutani et al. (2022), the mitochondrial boundary of EJ and WJ may have been maintained at the western edge of the Chugoku region from the last glacial period to the present. Therefore, EJ and WJ likely shared refugia during the glacial period, resulting in admixture. The admixed individuals may have spread to Shikoku and surrounding islands through the Seto Inland Sea, which covered a terrestrial and freshwater environment due to the lower sea level during the glacial period until 13,000 years ago between the western part of Chugoku and Shikoku regions (Yashima, 1994).

Commented [DR3]: Please note this region on the map in Figure 4.

Commented [DR4]: Please note this region on the map in Figure 4.

Commented [DR5]: Please refer to each image which may help in visualizing each one of these comparisons (e.g. Fig 4B, Fig S3, etc) int his and the next section.

Commented [DR6]: Please have this (region) notated somewhere on the map in Fig 4.

While the strait formation between the Chugoku and Kyushu region was 8,000 years ago (Yashima, 1994), later than between the Chugoku and Shikoku region, the admix~~tur~~ed individuals were identified in Shikoku but not in Kyushu, possibly suggesting ~~the~~ asymmetric introgression. Furthermore, th~~is~~e asymmetric introgression may have resulted in discordance in mtDNA and nuclear cline position between EJ and WJ, where the mitochondrial cline center is shifted about 40 km west compared to the nuclear cline center, with partially overlapping confidence intervals. The ~~dis~~incongruity of clines inferred from different sets of molecular markers is a common phenomenon of terrestrial vertebrate hybrid zones, including amphibians (e.g., Dufresnes et al., 2014; Arntzen et al., 2017; Sequeira et al., 2020). Prezygotic or postzygotic effects could explain the discordance in mtDNA and nuclear cline position. For prezygotic effects, sex-biased asymmetries (Toews & Brelsford, 2012) and an environmental gradient acting on mtDNA (Cheviron & Brumfield, 2009), and for the postzygotic effects, Haldane's rule (Haldane, 1922; Orr, 1997) and Dobzhansky–Muller incompatibilities (Dobzhansky, 1936; Muller, 1942) can produce discordance of mtDNA and nuclear cline~~s~~. Future field and genomic studies could test these hypotheses, revealing the factors that caused admixed individuals to spread mainly to the east of the mtDNA boundary at the time of secondary contact during the glacial period.

The width of the cline, including Shikoku, is wide, and using the above formula~~,~~ it ~~takes~~ would take 20,490 years to reach 161.8 km~~, while t~~The width of the cline, not including Shikoku, is 88.6 km~~, reaching~~ which would take 6,144 years to reach, suggesting that selection may not act in the Shikoku region, but in the Chugoku region. Furthermore, the range of present suitable habitats for EJ and WJ in Fukutani et al. (2022) was almost consistent with the actual distribution boundaries within the Chugoku region, indicating the possibility of exogenous environmental factors. However, the morphological differences between EJ and WJ ~~did~~ were not identifi~~ed~~ed~~y~~ in a previous study (Matsui, 1984). Moreover, the distribution of the admix~~tur~~ed individual in the Shikoku region suggests that EJ and WJ are the same species, notwithstanding the different degrees of admixture on the transect in the Chugoku and Shikoku region.

The toad population in Yakushima was once considered a different subspecies (Okada, 1928) but is now recognized to be the same species based on morphology (Matsui 1984). It supports a morphological classification that they are not monophyletic based on the mitochondrial phylogeny in the previous study (Fukutani et al., 2022) and not clustered in a single cluster in this study. There might have been interbreeding between Kyushu, Yakushima, and Tanegashima populations when the straits between Yakushima, Tanegashima, and Kagoshima were terrestrial during the glacial period (Ikehara, 1992). The geographic isolation after the last glacial period could have led to the deviation from isolation by distance.

Commented [DR7]: Please include a notation of this region in Figure 4.

Commented [DR8]: Please add all of these regions to the map in Figure 4.

The hybrid zone within *B. j. formosus*

We identified that the hybrid zone between NF and SF ~~was~~ as the widest in our study, which ~~is~~ was an expected result because of their recent evolutionary histories. The widespread gene flow and recent hybridization could indicate the absence of endogenous reproductive barriers between NF and SF. Furthermore, the mtDNA and SNPs clines between NF and SF had an almost concordant center, which could also suggest no selection (Toews & Brelsford, 2012). In contrast, the SNP cline~~s~~ was wider than the mitochondrial ~~one~~ cline across the transition between NF and SF, which ~~is the general case~~was due to a lower effective population size of mitochondrial DNA than the nuclear markers (Toews & Brelsford, 2012).

To reach the 170 km width of the SNP cline between NF and SF without selection, ~~I~~it ~~can be~~was calculated to ~~be~~ take 2,2,619 years ~~to reach the 170 km width of the SNP cline between NF and SF without selection~~, suggesting a prominent role for neutral processes. According to our previously predicted distributions during the glacial period, NF and SF could have shared their refugia around the southern Tohoku to northern Kanto regions. The expansion of distribution after the last glacial period probably led to widespread hybridization. An expansive hybrid zone consisting of late-generation hybrids and backcrosses is consistent overall with a prolonged period of neutral expansion. Though we did not find any asymmetry for the hybrid class assignment in the triangle plots, the results of the direction of migration were predominantly from SF to NF across the hybrid population (Fig. 6). Consequently, this hybrid zone probably leads to forming the hybrid swarm in NF populations in the future rather than the hybrid zone movement.

Commented [DR9]: Please indicate these regions on the map in Figure 4.

Commented [DR10]: I'm not sure what you're trying to say with this sentence. Perhaps rewording it for clarity would help.

Conclusion

In summary, we have presented the three hybrid zones, which were different in cline~~s~~ shapes. The populations with greater divergence had a sharper hybrid zone cline. These results in Japanese toads were consistent with other studies on anuran species (e.g., Dufresnes et al., 2018, 2020c). This is ~~E~~especially so for the most deeply diverged populations~~,~~ within *B. j. japonicus* and *B. j. formosus*, which had ~~a quite~~ sharp cline~~s,~~ suggesting the presence of strong selection (Mallet et al., 1990). This result contributes to resolving taxonomic confusion in Japanese toads. In addition, these results provide insights into the role of the hybrid zone on speciation and the processes that create and maintain biodiversity.

Commented [DR11]: These subspecies are not yet elevated, so I added the subspecies names for clarity here and in the sections above. If you would like to refer to them by these full-species names throughout the end of the Discussion and Conclusion, please make a note of it somewhere beforehand. Otherwise referring to "B. japonicus" would make the reader think of both subspecies as indicated throughout the first half of the manuscript.

Acknowledgments

We acknowledge K. Eto, I. Fukuyama, R. Fukuyama, S. Ikeda, K. Kimura, Y. Misawa, Y. Miyagata, T. Shimada, T. Sugahara, T. Sugihara, Y. Tahara, S. Tanabe, A. Tominaga, N. Yoshikawa, and many more collaborators for collecting samples. We thank N. Yoshikawa and Y. Fuke for helping to conduct Mig-seq sequences and analyses. We also thank our laboratory members for helping with specimen processing and molecular experiments. Finally, we thank the reviewers for their valuable comments.

References

Abbott R, Albach D, Ansell S, Arntzen JW, Baird SJE, Bierne N, Boughman J, Brelsford A, Buerkle CA, Buggs R, Butlin RK, Dieckmann U, Eroukhmanoff F, Grill A, Cahan SH, Hermansen JS, Hewitt G, Hudson AG, Jiggins C, Jones J, Keller B, Marczewski T, Mallet J, Martinez-Rodriguez P, Möst M, Mullen S, Nichols R, Nolte AW, Parisod C, Pfennig K, Rice AM, Ritchie MG, Seifert B, Smadja CM, Stelkens R, Szymura JM, Väinölä R, Wolf JBW, Zinner D. 2013. Hybridization and speciation. *Journal of Evolutionary Biology* 26:229–246. DOI: 10.1111/j.1420-9101.2012.02599.x.

Anderson DR, Burnham KP. 2002. Avoiding pitfalls when using information-theoretic methods. *The Journal of Wildlife Management* 66:912. DOI: 10.2307/3803155.

Arntzen JW, Trujillo T, Butôt R, Vrieling K, Schaap O, Gutiérrez-Rodríguez J, Martínez-Solano I. 2016. Concordant morphological and molecular clines in a contact zone of the Common and Spined toad (*Bufo bufo* and *B. spinosus*) in the northwest of France. *Frontiers in Zoology* 13:52. DOI: 10.1186/s12983-016-0184-7.

Arntzen JW, Vries W, Canestrelli D, Martínez-Solano I. 2017. Hybrid zone formation and contrasting outcomes of secondary contact over transects in common toads. *Molecular Ecology* 26:5663–5675. DOI: 10.1111/mec.14273.

Barton NH, Gale K. 1993. Genetic analysis of hybrid zones. In: *Hybrid Zones and the Evolutionary Process*. New York: Oxford University Press, 13–45.

Barton NH, Hewitt GM. 1985. Analysis of hybrid zones. *Annual Review of Ecology and Systematics* 16:113–148. DOI: 10.1146/annurev.es.16.110185.000553.

Bouckaert R, Vaughan TG, Barido-Sottani J, Duchêne S, Fourment M, Gavryushkina A, Heled J, Jones G, Kühnert D, Maio ND, Matschiner M, Mendes FK, Müller NF, Ogilvie HA, Plessis L du, Popinga A, Rambaut A, Rasmussen D, Siveroni I, Suchard MA, Wu C-H, Xie D, Zhang C, Stadler T, Drummond AJ. 2019. BEAST 2.5: an advanced software platform for Bayesian evolutionary analysis. *PLoS Computational Biology* 15:e1006650. DOI: 10.1371/journal.pcbi.1006650.

Bryant D, Bouckaert R, Felsenstein J, Rosenberg NA, RoyChoudhury A. 2012. Inferring species trees directly from biallelic genetic markers: bypassing gene trees in a full coalescent analysis. *Molecular Biology and Evolution* 29:1917–1932. DOI: 10.1093/molbev/mss086.

Butlin RK, Smadja CM. 2018. Coupling, reinforcement, and speciation. *The American Naturalist* 191:155–172. DOI: 10.1086/695136.

Cavalli-Sforza LL. 1966. Population structure and human evolution. *Proceedings of the Royal Society of London. Series B. Biological Sciences* 164:362–379. DOI: 10.1098/rspb.1966.0038.

Caye K, Deist TM, Martins H, Michel O, François O. 2016. TESS3: fast inference of spatial population structure and genome scans for selection. *Molecular Ecology Resources* 16:540–548. DOI: 10.1111/1755-0998.12471.

Caye K, Jay F, Michel O, François O. 2018. Fast inference of individual admixture coefficients using geographic data. *The Annals of Applied Statistics* 12:586–608. DOI: 10.1214/17-aoas1106.

Chen S, Zhou Y, Chen Y, Gu J. 2018. fastp: an ultra-fast all-in-one FASTQ preprocessor. *Bioinformatics* 34:i884–i890. DOI: 10.1093/bioinformatics/bty560.

Cheviron ZA, Brumfield RT. 2009. Migration-Selection Balance and Local Adaptation of Mitochondrial Haplotypes in Rufous-Collared Sparrows (*Zonotrichia capensis*) Along an Elevational Gradient. *Evolution* 63:1593–1605. DOI: 10.1111/j.1558-5646.2009.00644.x.

Colliard C, Sicilia A, Turrisi GF, Arculeo M, Perrin N, Stöck M. 2010. Strong reproductive barriers in a narrow hybrid zone of West-Mediterranean green toads (Bufo viridis subgroup) with Plio-Pleistocene divergence. *BMC Evolutionary Biology* 10:232–232. DOI: 10.1186/1471-2148-10-232.

Derryberry EP, Derryberry GE, Maley JM, Brumfield RT. 2014. hzar: hybrid zone analysis using an R software package. *Molecular Ecology Resources* 14:652–663. DOI: 10.1111/1755-0998.12209.

Dobzhansky T. 1936. Studies on hybrid sterility. II. Localization of sterility factors in Drosophila pseudoobscura hybrids. *Genetics* 21:113–135. DOI: 10.1093/genetics/21.2.113.

Dufresnes C, Bonato L, Novarini N, Betto-Colliard C, Perrin N, Stöck M. 2014. Inferring the degree of incipient speciation in secondary contact zones of closely related lineages of Palearctic green toads (*Bufo viridis* subgroup). *Heredity* 113:9. DOI: 10.1038/hdy.2014.26.

687 Dufresnes C, Brelsford A, Jeffries DL, Mazepa G, Suchan T, Canestrelli D, Nicieza A,
688 Fumagalli L, Dubey S, Martínez-Solano I, Litvinchuk SN, Vences M, Perrin N, Crochet
689 P-A. 2021. Mass of genes rather than master genes underlie the genomic architecture of
690 amphibian speciation. *Proceedings of the National Academy of Sciences*
691 118:e2103963118. DOI: 10.1073/pnas.2103963118.
692 Dufresnes C, Litvinchuk SN. 2021. Diversity, distribution and molecular species delimitation in
693 frogs and toads from the Eastern Palaearctic. *Zoological Journal of the Linnean Society*
694 XX:1–66. DOI: 10.1093/zoolinnean/zlab083.
695 Dufresnes C, Litvinchuk SN, Rozenblut-Kościsty B, Rodrigues N, Perrin N, Crochet P, Jeffries
696 DL. 2020a. Hybridization and introgression between toads with different sex
697 chromosome systems. *Evolution Letters* 4:444–456. DOI: 10.1002/evl3.191.
698 Dufresnes C, Lymberakis P, Kornilios P, Savary R, Perrin N, Stöck M. 2018. Phylogeography of
699 Aegean green toads (*Bufo viridis* subgroup): continental hybrid swarm vs. insular
700 diversification with discovery of a new island endemic. *BMC Evolutionary Biology* 18:1–
701 12. DOI: 10.1186/s12862-018-1179-0.
702 Dufresnes C, Nicieza AG, Litvinchuk SN, Rodrigues N, Jeffries DL, Vences M, Perrin N,
703 Martínez-Solano Í. 2020b. Are glacial refugia hotspots of speciation and cytonuclear
704 discordances? Answers from the genomic phylogeography of Spanish common frogs.
705 *Molecular Ecology* 29:986–1000. DOI: 10.1111/mec.15368.
706 Dufresnes C, Pribille M, Alard B, Gonçalves H, Amat F, Crochet P-A, Dubey S, Perrin N,
707 Fumagalli L, Vences M, Martínez-Solano I. 2020c. Integrating hybrid zone analyses in
708 species delimitation: lessons from two anuran radiations of the Western Mediterranean.
709 *Heredity* 124:423–438. DOI: 10.1038/s41437-020-0294-z.
710 Evanno G, Regnaut S, Goudet J. 2005. Detecting the number of clusters of individuals using the
711 software structure: a simulation study. *Molecular Ecology* 14:2611–2620. DOI:
712 10.1111/j.1365-294x.2005.02553.x.
713 Fukutani K, Matsui M, Tran DV, Nishikawa K. 2022. Genetic diversity and demography of *Bufo*
714 *japonicus* and *B. torrenticola* (Amphibia: Anura: Bufonidae) influenced by the
715 Quaternary climate. *PeerJ* 10:e13452. DOI: 10.7717/peerj.13452.
716 Gargiulo R, Kull T, Fay MF. 2021. Effective double-digest RAD sequencing and genotyping
717 despite large genome size. *Molecular Ecology Resources* 21:1037–1055. DOI:
718 10.1111/1755-0998.13314.
719 Gompert Z, Buerkle CA. 2010. INTROGRESS: a software package for mapping components of
720 isolation in hybrids. *Molecular Ecology Resources* 10:378–384. DOI: 10.1111/j.1755-
721 0998.2009.02733.x.
722 Haldane JBS. 1922. Sex ratio and unisexual sterility in hybrid animals. *Journal of Genetics*
723 12:101–109. DOI: 10.1007/bf02983075.
724 Harrison RG, Larson EL. 2014. Hybridization, Introgression, and the Nature of Species
725 Boundaries. *Journal of Heredity* 105:795–809. DOI: 10.1093/jhered/esu033.
726 Hastings WK. 1970. Monte Carlo sampling methods using Markov chains and their applications.
727 *Biometrika* 57:97. DOI: 10.2307/2334940.
728 Hewitt GM. 1988. Hybrid zones-natural laboratories for evolutionary studies. *Trends in Ecology*
729 *& Evolution* 3:158–167. DOI: 10.1016/0169-5347(88)90033-x.
730 Hickerson MJ, Meyer CP, Moritz C. 2006. DNA barcoding will often fail to discover new
731 animal species over broad parameter space. *Systematic Biology* 55:729–739. DOI:
732 10.1080/10635150600969898.

Hohenlohe PA, Amish SJ, Catchen JM, Allendorf FW, Luikart G. 2011. Next-generation RAD sequencing identifies thousands of SNPs for assessing hybridization between rainbow and westslope cutthroat trout. *Molecular Ecology Resources* 11:117–122. DOI: 10.1111/j.1755-0998.2010.02967.x.

Igawa T, Kurabayashi A, Nishioka M, Sumida M. 2006. Molecular phylogenetic relationship of toads distributed in the Far East and Europe inferred from the nucleotide sequences of mitochondrial DNA genes. *Molecular Phylogenetics and Evolution* 38:250–260. DOI: 10.1016/j.ympev.2005.09.003.

Ikehara K. 1992. Formation of duned sand bodies in the Osumi Strait, south of Kyushu, Japan. *Journal of the Sedimentological Society of Japan* 36:37–45. DOI: 10.14860/jssj1972.36.37.

Jombart T. 2008. *adegenet*: a R package for the multivariate analysis of genetic markers. *Bioinformatics* 24:1403–1405. DOI: 10.1093/bioinformatics/btn129.

Jombart T, Ahmed I. 2011. *adegenet 1.3-1*: new tools for the analysis of genome-wide SNP data. *Bioinformatics* 27:3070–3071. DOI: 10.1093/bioinformatics/btr521.

Jombart T, Devillard S, Balloux F. 2010. Discriminant analysis of principal components: a new method for the analysis of genetically structured populations. *BMC Genetics* 11:94–94. DOI: 10.1186/1471-2156-11-94.

Key KHL. 1968. The concept of stasipatric speciation. *Systematic Biology* 17:14–22. DOI: 10.1093/sysbio/17.1.14.

Kopelman NM, Mayzel J, Jakobsson M, Rosenberg NA, Mayrose I. 2015. Clumpak: a program for identifying clustering modes and packaging population structure inferences across K. *Molecular Ecology Resources* 15:1179–1191. DOI: 10.1111/1755-0998.12387.

Kusano T, Maruyama K, Kaneko S. 1995. Post-breeding dispersal of the Japanese toad, *Bufo japonicus formosus*. *Journal of Herpetology* 29:633. DOI: 10.2307/1564755.

Li H, Handsaker B, Wysoker A, Fennell T, Ruan J, Homer N, Marth G, Abecasis G, Durbin R, Subgroup 1000 Genome Project Data Processing. 2009. The sequence alignment/map format and SAMtools. *Bioinformatics* 25:2078–2079. DOI: 10.1093/bioinformatics/btp352.

Li Y, Liu J. 2018. StructureSelector: A web-based software to select and visualize the optimal number of clusters using multiple methods. *Molecular Ecology Resources* 18:176–177. DOI: 10.1111/1755-0998.12719.

Mallet J, Barton N, Lamas G, Santisteban J, Muedas M, Eeley H. 1990. Estimates of selection and gene flow from measures of cline width and linkage disequilibrium in heliconius hybrid zones. *Genetics* 124:921–936. DOI: 10.1093/genetics/124.4.921.

Marcus J, Ha W, Barber RF, Novembre J. 2021. Fast and flexible estimation of effective migration surfaces. *eLife* 10:e61927. DOI: 10.7554/elife.61927.

Matsui M. 1984. Morphometric variation analyses and revision of the Japanese toads (Genus *Bufo*, Bufonidae). *Contributions from the Biological Laboratory, Kyoto University* 26:209–428.

Matsui M, Maeda N. 2018. *Encyclopedia of Japanese frogs*. Tokyo: Bun-ichi Sogo Shuppan.

Matsui M, Okawa H, Nishikawa K, Aoki G, Eto K, Yoshikawa N, Tanabe S, Misawa Y, Tominaga A. 2019. Systematics of the widely distributed Japanese clouded salamander, *Hynobius nebulosus* (Amphibia: Caudata: Hynobiidae), and its closest relatives. *Current Herpetology* 38:32–90. DOI: 10.5358/hsj.38.32.

Metropolis N, Rosenbluth AW, Rosenbluth MN, Teller AH, Teller E. 1953. Equation of State Calculations by Fast Computing Machines. *The Journal of Chemical Physics* 21:1087–1092. DOI: 10.1063/1.1699114.

Milne RI, Abbott RJ. 2008. Reproductive isolation among two interfertile *Rhododendron* species: low frequency of post-F1 hybrid genotypes in alpine hybrid zones. *Molecular Ecology* 17:1108–1121. DOI: 10.1111/j.1365-294x.2007.03643.x.

Miura I. 1995. The late replication banding patterns of chromosomes are highly conserved in the genera *Rana*, *Hyla*, and *Bufo* (Amphibia: Anura). *Chromosoma* 103:567–574. DOI: 10.1007/bf00355322.

Muller HJ. 1942. Isolating mechanisms, evolution, and temperature. *Biological Symposia*:71–125.

Mussmann SM, Douglas MR, Chafin TK, Douglas ME. 2019. BA3-SNPs: Contemporary migration reconfigured in BayesAss for next-generation sequence data. *Methods in Ecology and Evolution* 10:1808–1813. DOI: 10.1111/2041-210x.13252.

Okada Y. 1928. Notes on Japanese frogs. *Annotationes Zoologicae Japonenses* 11:269–277.

Orr HA. 1997. Haldane's Rule. *Annual Review of Ecology and Systematics* 28:195–218. DOI: 10.1146/annurev.ecolsys.28.1.195.

Petkova D, Novembre J, Stephens M. 2016. Visualizing spatial population structure with estimated effective migration surfaces. *Nature Genetics* 48:94–100. DOI: 10.1038/ng.3464.

Pritchard JK, Stephens M, Donnelly P. 2000. Inference of population structure using multilocus genotype data. *Genetics* 155:945–959. DOI: 10.1093/genetics/155.2.945.

Puechmaille SJ. 2016. The program structure does not reliably recover the correct population structure when sampling is uneven: subsampling and new estimators alleviate the problem. *Molecular Ecology Resources* 16:608–627. DOI: 10.1111/1755-0998.12512.

Rambaut A, Drummond AJ, Xie D, Baele G, Suchard MA. 2018. Posterior summarization in Bayesian phylogenetics using Tracer 1.7. *Systematic Biology* 67:901–904. DOI: 10.1093/sysbio/syy032.

R Core Team (2022). R: A language and environment for statistical computing. *R Foundation for Statistical Computing*, Vienna, Austria. URL https://www.R-project.org/.

Riemsdijk I van, Arntzen JW, Bucciarelli GM, McCartney-Melstad E, Rafajlović M, Scott PA, Toffelmier E, Shaffer HB, Wielstra B. 2023. Two transects reveal remarkable variation in gene flow on opposite ends of a European toad hybrid zone. *Heredity*:1–10. DOI: 10.1038/s41437-023-00617-6.

RStudio Team (2022). RStudio: Integrated Development Environment for R. *RStudio, PBC, Boston, MA* URL http://www.rstudio.com/.

Rochette NC, Rivera-Colón AG, Catchen JM. 2019. Stacks 2: Analytical methods for paired-end sequencing improve RADseq-based population genomics. *Molecular Ecology* 28:4737–4754. DOI: 10.1111/mec.15253.

Scordato ESC, Wilkins MR, Semenov G, Rubtsov AS, Kane NC, Safran RJ. 2017. Genomic variation across two barn swallow hybrid zones reveals traits associated with divergence in sympatry and allopatry. *Molecular Ecology* 26:5676–5691. DOI: 10.1111/mec.14276.

Sequeira F, Bessa-Silva A, Tarroso P, Sousa-Neves T, Vallinoto M, Gonçalves H, Martínez-Solano I. 2020. Discordant patterns of introgression across a narrow hybrid zone between two cryptic lineages of an Iberian endemic newt. *Journal of Evolutionary Biology* 33:202–216. DOI: 10.1111/jeb.13562.

824 Servedio MR, Hermisson J. 2020. The evolution of partial reproductive isolation as an adaptive
825 optimum. *Evolution* 74:4–14. DOI: 10.1111/evo.13880.
826 Slager DL, Epperly KL, Ha RR, Rohwer S, Wood C, Hemert C, Klicka J. 2020. Cryptic and
827 extensive hybridization between ancient lineages of American crows. *Molecular Ecology*
828 29:956–969. DOI: 10.1111/mec.15377.
829 Stamatakis A. 2014. RAxML version 8: a tool for phylogenetic analysis and post-analysis of
830 large phylogenies. *Bioinformatics* 30:1312–1313. DOI: 10.1093/bioinformatics/btu033.
831 Stöck M, Moritz C, Hickerson M, Frynta D, Dujsebayeva T, Eremchenko V, Macey JR,
832 Papenfuss TJ, Wake DB. 2006. Evolution of mitochondrial relationships and
833 biogeography of Palearctic green toads (*Bufo viridis* subgroup) with insights in their
834 genomic plasticity. *Molecular Phylogenetics and Evolution* 41:663–689. DOI:
835 10.1016/j.ympev.2006.05.026.
836 Suyama Y, Hirota SK, Matsuo A, Tsunamoto Y, Mitsuyuki C, Shimura A, Okano K. 2022.
837 Complementary combination of multiplex high-throughput DNA sequencing for
838 molecular phylogeny. *Ecological Research* 37:171–181. DOI: 10.1111/1440-1703.12270.
839 Suyama Y, Matsuki Y. 2015. MIG-seq: an effective PCR-based method for genome-wide single-
840 nucleotide polymorphism genotyping using the next-generation sequencing platform.
841 *Scientific Reports* 5:srep16963. DOI: 10.1038/srep16963.
842 Szymura JM, Barton NH. 1986. Genetic analysis of a hybrid zone between the fire-bellied toads
843 *Bombina bombina* and *B. variegata*, near Cracow in Southern Poland. *Evolution*
844 40:1141–1159. DOI: 10.1111/j.1558-5646.1986.tb05740.x.
845 Szymura JM, Barton NH. 1991. The genetic structure of the hybrid zone between the fire-bellied
846 toads *Bombina bombina* and *B. variegata*: comparisons between transects and between
847 loci. *Evolution* 45:237–261. DOI: 10.1111/j.1558-5646.1991.tb04400.x.
848 Takata K, Iwase F, Iguchi A, Yuasa H, Taninaka H, Iwasaki N, Uda K, Suzuki T, Nonaka M,
849 Kikuchi T, Yasuda N. 2021. Genome-wide SNP data revealed notable spatial genetic
850 structure in the deep-sea precious coral *Corallium japonicum*. *Frontiers in Marine*
851 *Science* 8:667481. DOI: 10.3389/fmars.2021.667481.
852 Toews DPL, Brelsford A. 2012. The biogeography of mitochondrial and nuclear discordance in
853 animals. *Molecular Ecology* 21:3907–3930. DOI: 10.1111/j.1365-294x.2012.05664.x.
854 Tominaga A, Matsui M, Yoshikawa N, Eto K, Nishikawa K. 2018. Genomic displacement and
855 shift of the hybrid zone in the Japanese fire-bellied newt. *Journal of Heredity* 109:232–
856 242. DOI: 10.1093/jhered/esx085.
857 Toyama KS, Crochet P, Leblois R. 2020. Sampling schemes and drift can bias admixture
858 proportions inferred by structure. *Molecular Ecology Resources* 20:1769–1785. DOI:
859 10.1111/1755-0998.13234.
860 Vähä J-P, Primmer CR. 2006. Efficiency of model-based Bayesian methods for detecting hybrid
861 individuals under different hybridization scenarios and with different numbers of loci.
862 *Molecular Ecology* 15:63–72. DOI: 10.1111/j.1365-294x.2005.02773.x.
863 Vasimuddin M, Misra S, Li H, Aluru S. 2024. Efficient architecture-aware acceleration of BWA-
864 MEM for multicore systems. In: 2019 IEEE International Parallel and Distributed
865 Processing Symposium (IPDPS). Rio de Janeiro, Brazil, 314–324. DOI:
866 10.1109/ipdps.2019.00041.
867 Watanabe K, Tabata R, Nakajima J, Kobayakawa M, Matsuda M, Takaku K, Hosoya K, Ohara
868 K, Takagi M, Jang-Liaw N-H. 2020. Large-scale hybridization of Japanese populations

of Hinamoroko, *Aphyocypris chinensis*, with *A. kikuchii* introduced from Taiwan. *Ichthyological Research* 67:361–374. DOI: 10.1007/s10228-019-00730-9.

Willis SC, Hollenbeck CM, Puritz JB, Gold JR, Portnoy DS. 2017. Haplotyping RAD loci: an efficient method to filter paralogs and account for physical linkage. *Molecular Ecology Resources* 17:955–965. DOI: 10.1111/1755-0998.12647.

Wilson GA, Rannala B. 2003. Bayesian inference of recent migration rates using multilocus genotypes. *Genetics* 163:1177–1191. DOI: 10.1093/genetics/163.3.1177.

Wu C. 2001. The genic view of the process of speciation. *Journal of Evolutionary Biology* 14:851–865. DOI: 10.1046/j.1420-9101.2001.00335.x.

Yanchukov A, Hofman S, Szymura JM, Mezhzherin SV, Morozov-Leonov SY, Barton NH, Nrnberger B. 2006. Hybridization of *Bombina bombina* and *B. variegata* (Anura, Discoglossidae) at a sharp ecotone in western Ukraine: comparisons across transects and over time. *Evolution* 60:583–600. DOI: 10.1554/04-739.1.

Yashima K. 1994. A geomorphological study of the caldrons in the Seto inland sea. *Report of Hydrographic Researches*:237–327.

Zhao H, Beck B, Fuller A, Peatman E. 2020. EasyParallel: A GUI platform for parallelization of STRUCTURE and NEWHYBRIDS analyses. *Plos One* 15:e0232110. DOI: 10.1371/journal.pone.0232110.

Figure 1

Population structure using (A) DAPC, (B) Structure, and (C) PCA based on SNPs datasets, dataset i) for DAPC and PCA, and dataset i)-2 for Structure.

The four different genetic clusters, northern *B. j. formosus* (NF), southern *B. j. formosus* (SF), eastern *B. j. japonicus* (EJ), western *B. j. japonicus* (WJ), are displayed with *B. torrenticola*. (A) DAPC plot shows the best fit for $K = 5$ clusters. The axes represent the first two linear discriminants (LD), and the dots represent individuals colored by their groups in DAPC. (B) Structure bar plots show individual ancestry to the five clusters ($K = 5$). (C) PC1 and PC2 are plotted. Each dot corresponds to an individual colored according to their genetic cluster found in DAPC. The first axis distinguishes *B. j. formosus* and *B. j. japonicus*, and the second axis distinguishes *B. japonicus* and *B. torrenticola* and reflects intraspecific structure within *B. japonicus*.

Figure 1B: While it is clear which sampled are assigned to B. torrenticola, it is unclear which samples belong to the other subspecies populations. It would be useful to see which samples have admixture, especially in the clades which you would l…

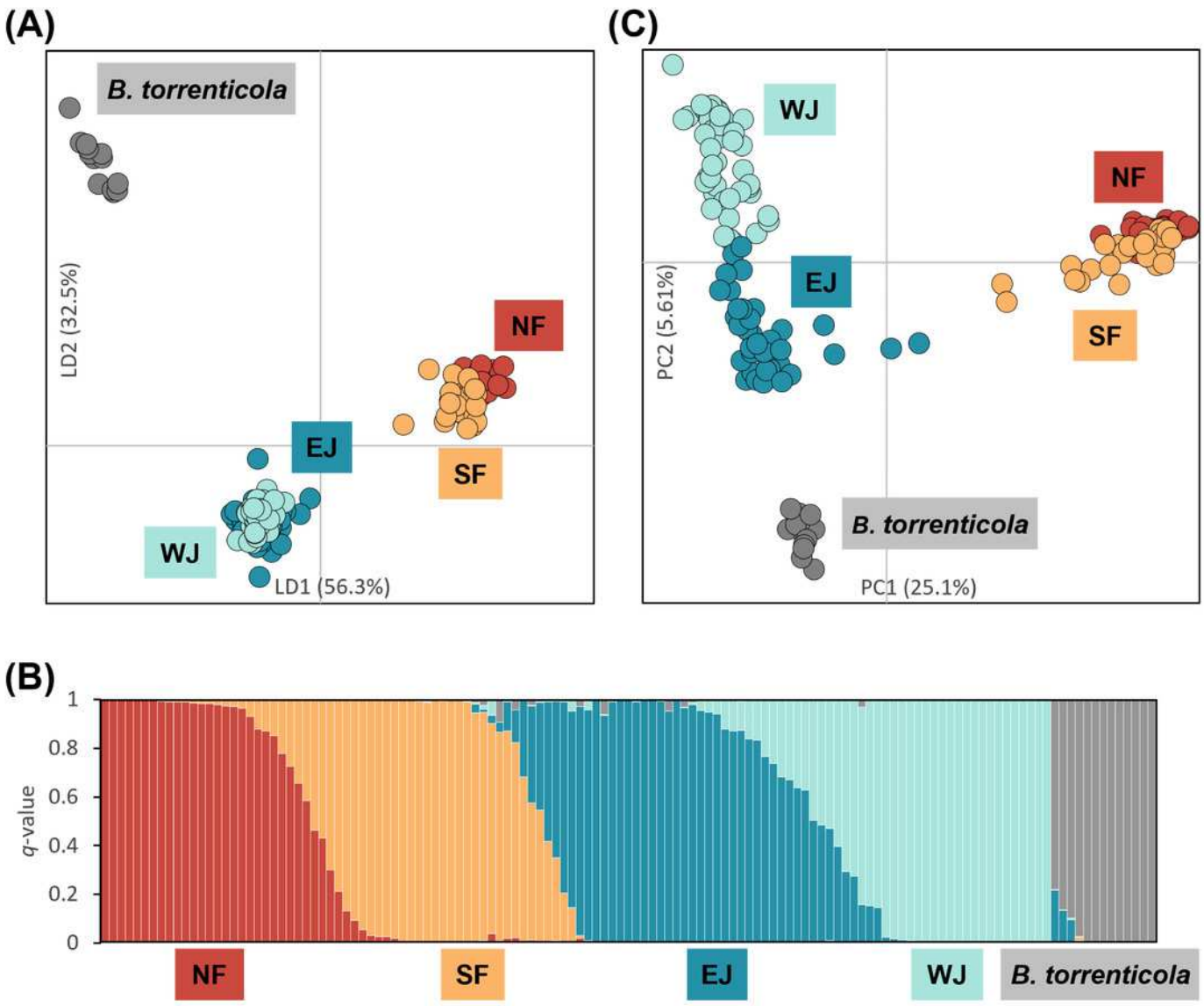
(A)
B. torrenticola
NF
EJ
SF
WJ
LD2 (32.5%)
LD1 (56.3%)
(C)
WJ
NF
EJ
SF
B. torrenticola
PC2 (5.61%)
PC1 (25.1%)
(B)
1
0.8
0.6
0.4
0.2
0
q-value
NF
SF
EJ
WJ
B. torrenticola

Figure 2

(A) Densitree diagram representing the species tree obtained from SNAPP using SNPs. (B) The phylogenetic tree using mitochondrial cytochrome *b* sequences.

(A) All nodes were supported by posterior probabilities of 1.0. (B) Asterisks on each node indicate bootstrap supports are more than 85%.

Figure 2B: There are no asterisks on any of the nodes.

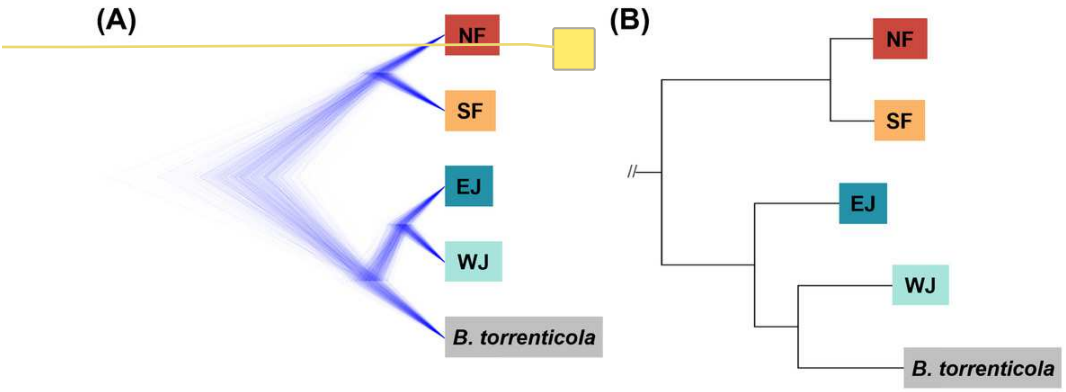

Figure 3

Effective migration rates for the lowest cross-validation lambda estimated by FEEMS (Fast Estimation of Effective Migration Surfaces) using dataset ii).

The figure shows the fitted parameters in the log scale, with lower effective migration shown in orange and higher effective migration shown in blue. Dots represent individuals.

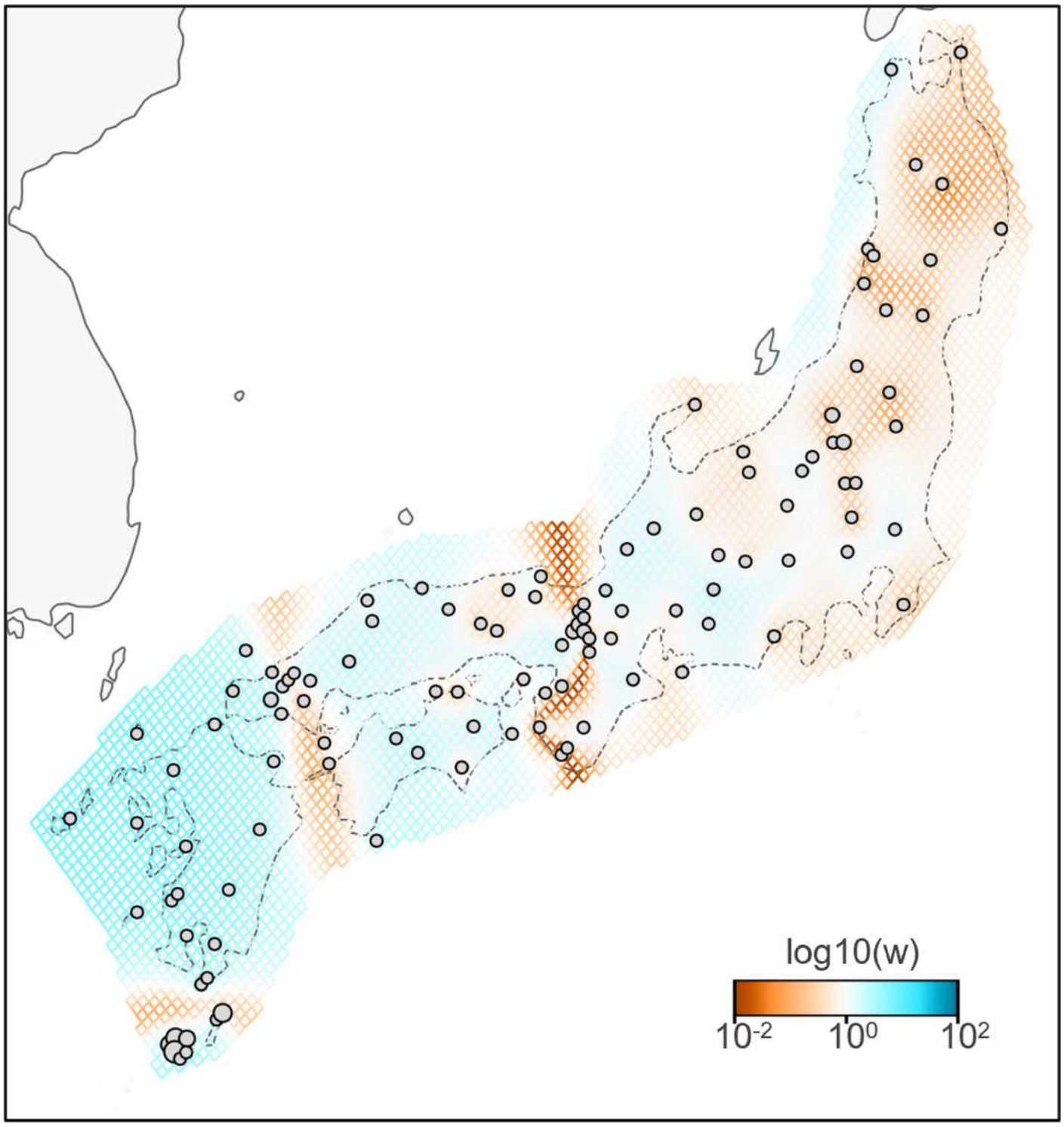
log10(w)
10-2
100
102

Figure 4

Maps showing sampling localities with pie charts for three different contact zone of sub-datasets, (A) SF–EJ, (B) NF–SF, and (C) EJ–WJ.

Pie charts show the *q*-values inferred by the Structure program for each individual. The dotted lines indicate the baselines used for *hzar*.

Figure 4: It would be useful to add some geographic context to these maps – e.g., adding the names of island/regions or an inset with a map of the larger geographic…

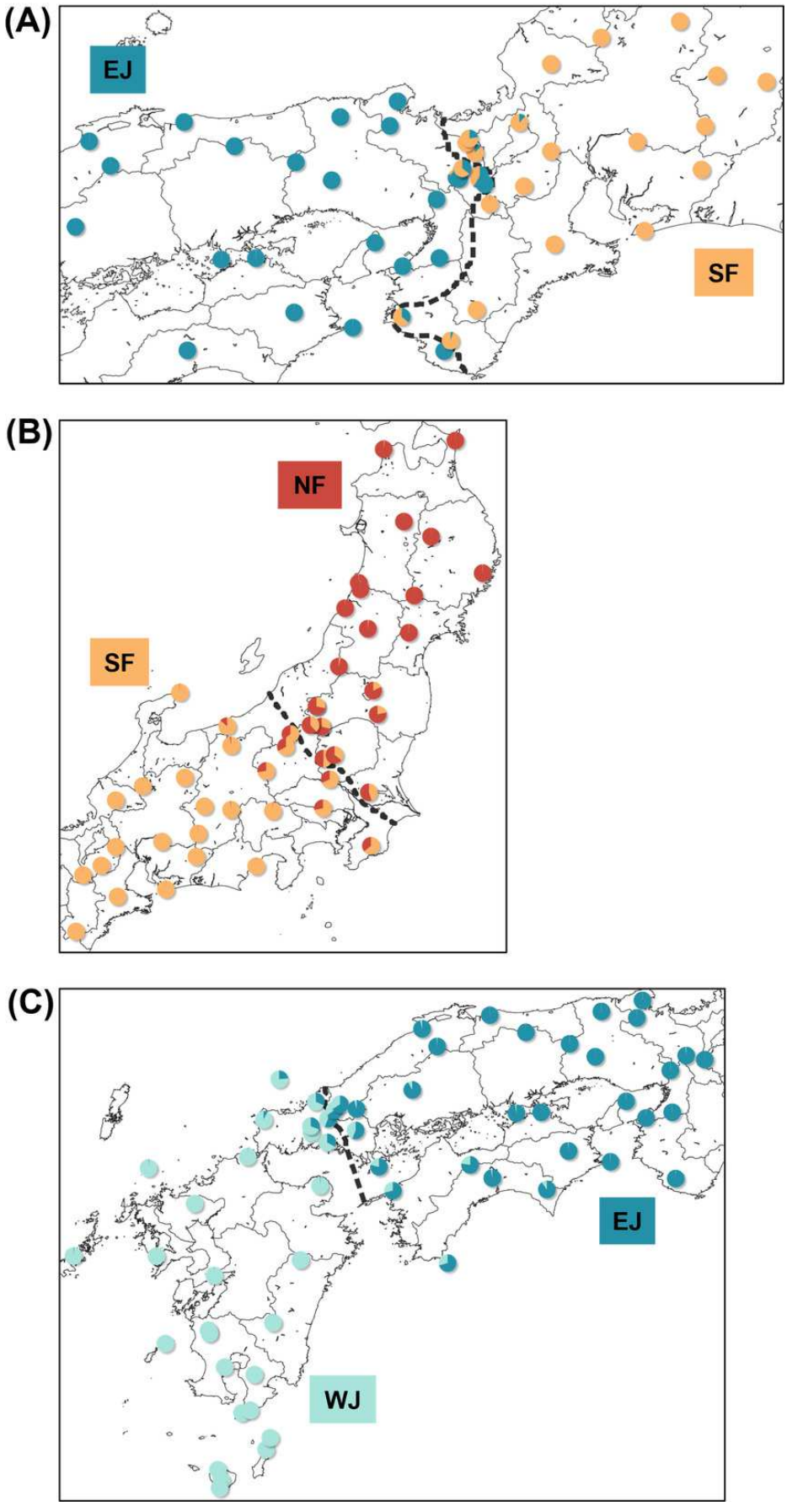
(A)
EJ
SF
(B)
NF
SF
(C)
EJ
WJ

Figure 5

The maximum-likelihood clines fitting on nuclear genomic average ancestry and mitochondrial allele frequencies along three different transect of sub-datasets, (A) SF–EJ, (B) NF–SF, and (C) EJ–WJ.

The grey areas show the 95% credible cline region. The x-axis represents distances (km) from the baselines shown in Fig. 4. Crosses indicate the observed values for individuals.

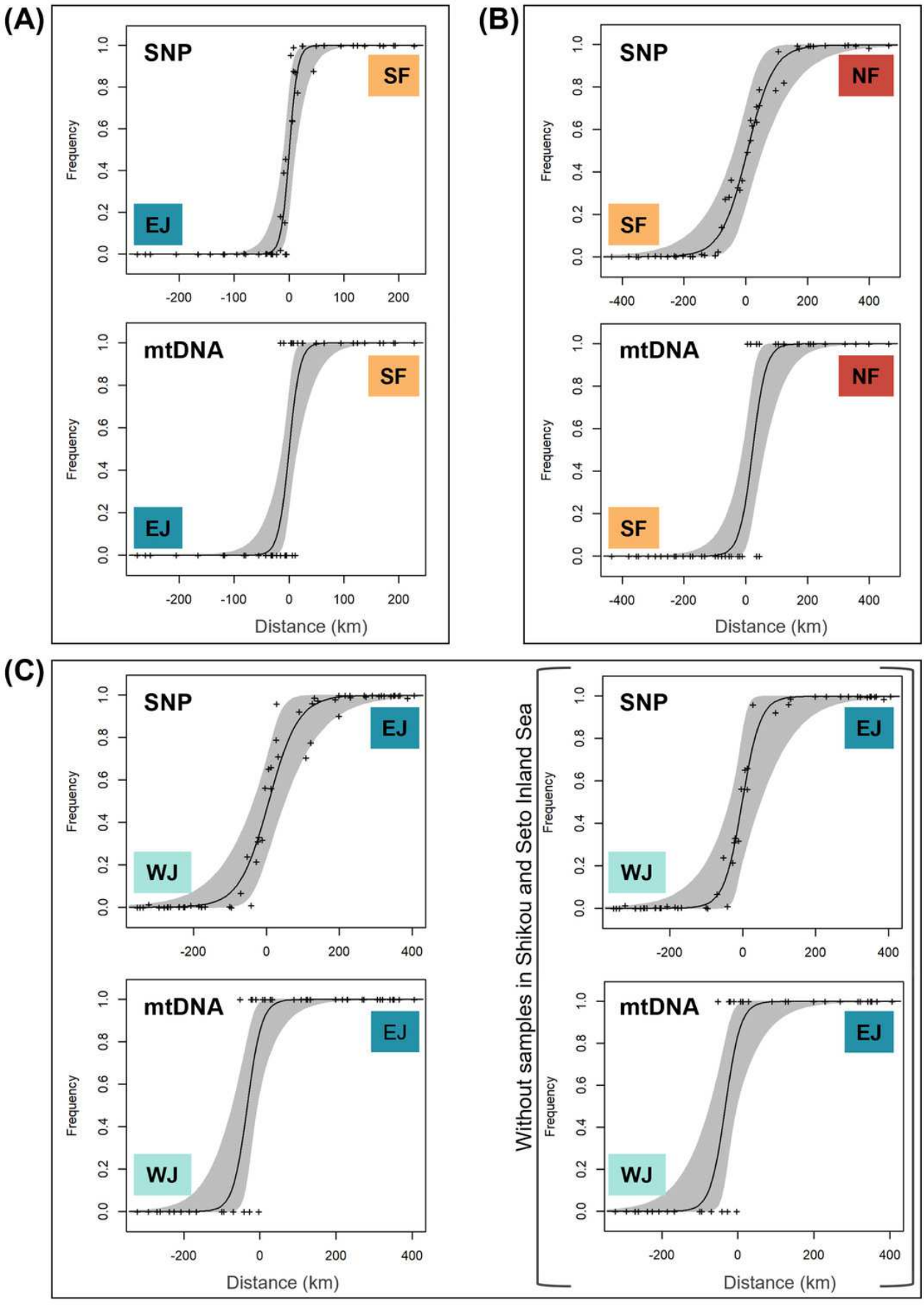
(A)
SNP
SF
EJ
mtDNA
SF
EJ
Frequency
Distance (km)
(B)
SNP
NF
SF
mtDNA
NF
SF
Frequency
Distance (km)
(C)
SNP
EJ
WJ
mtDNA
EJ
WJ
Frequency
Distance (km)
Without samples in Shikou and Seto Inland Sea
SNP
EJ
WJ
mtDNA
EJ
WJ
Frequency
Distance (km)

Figure 6

Triangle plots of the hybrid index versus heterozygosity of individuals based on selected ancestry-informative SNP markers (*F*st = 1) for sub-datasets, (A) SF–EJ, (B) NF–SF, and (C) EJ–WJ.

Individual with intermediate hybrid indices (> 0.25 and < 0.75) and high heterozygosity (≥ 0.5) was considered as recent-generation hybrid (a gray square), and those with intermediate hybrid indices (> 0.25 and < 0.75) and low heterozygosity (< 0.5) as later-generation hybrids (gray triangles). Those with low hybrid indices (≤ 0.25 or ≥ 0.75) were considered as backcross to one or the other parental type (triangles colored by parental assignments). Each colored circle indicates the pure individuals.

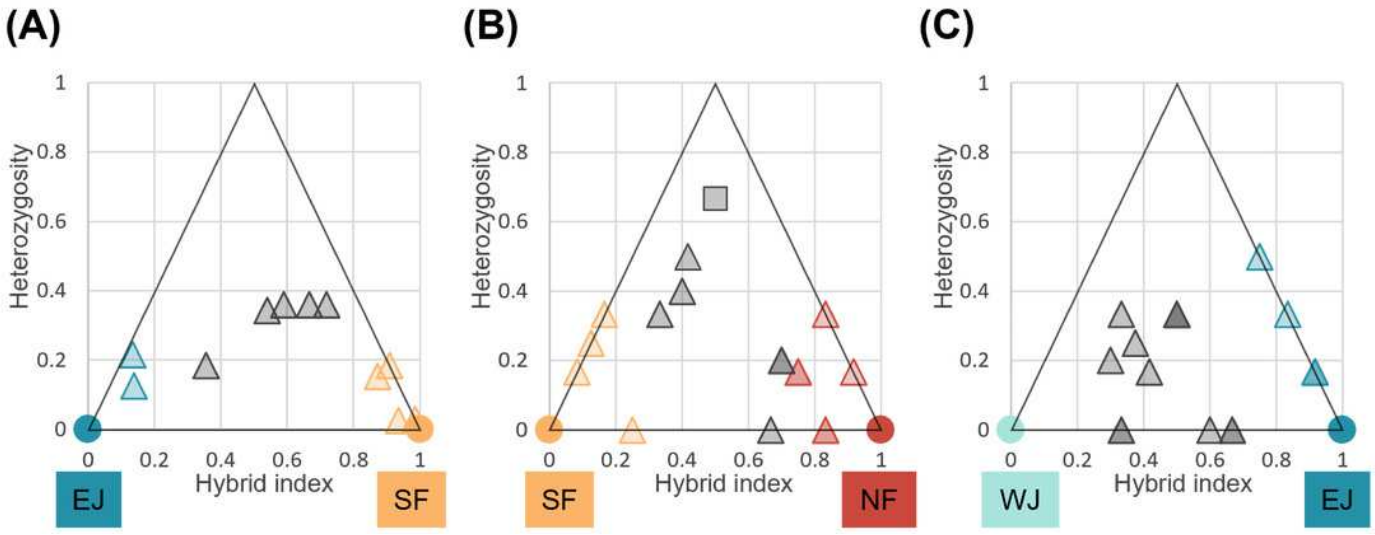

Table 1 (on next page)

Estimates of migrants from BayesAss3-SNPs analyses between population clusters, (A) SF–EJ, (B) NF–SF, and (C) EJ–WJ.

The row headers represent the populations into where the individuals migrated, and the column headers represent the populations from where the migrant derived. Standard deviations of the values are given in parentheses.

(A)

		Migration from		
		parental NF	Hybrid	parental SF
Migration into	parental NF	0.9407 (0.0349)	0.0355 (0.0290)	0.0238 (0.0221)
	Hybrid	0.0152 (0.0145)	0.9262 (0.0293)	0.0586 (0.0269)
	parental SF	0.0167 (0.0158)	0.0167 (0.0158)	0.9667 (0.0218)

(B)

		Migration from		
		parental SF	Hybrid	parental EJ
Migration into	parental SF	0.9607 (0.0253)	0.0196 (0.0185)	0.0196 (0.0185)
	Hybrid	0.1667 (0.0431)	0.7619 (0.0389)	0.0714 (0.0353)
	parental EJ	0.0133 (0.0128)	0.0133 (0.0128)	0.9733 (0.0178)

(C)

		Migration from		
		parental EJ	Hybrid	parental WJ
Migration into	parental EJ	0.9683 (0.0209)	0.0133 (0.0151)	0.0159 (0.0152)
	Hybrid	0.0725 (0.0280)	0.8013 (0.0340)	0.1262 (0.0337)
	parental WJ	0.0139 (0.0133)	0.0139 (0.0133)	0.9722 (0.0184)